The Astrophysical Journal, 603:322–329, 2004 March 1

THE INABILITY OF STEADY-FLOW MODELS TO EXPLAIN THE EXTREME-ULTRAVIOLET CORONAL LOOPS

S. Patsourakos[1] and J. A. Klimchuk
Naval Research Laboratory, Space Science Division, Washington, DC 20375; patsourakos@nrl.navy.mil

and

P. J. MacNeice
Physics and Atmospheric Science Department, Drexel University, Philadelphia, PA 19104
Received 2003 August 13; accepted 2003 November 17

ABSTRACT

Recent observations from the *Transition Region and Coronal Explorer* (*TRACE*) and the EUV Imaging Telescope (EIT) show that warm ($T \approx 1$–1.5 MK) EUV coronal loops in active regions generally have enhanced densities, enhanced pressure scale heights, and flat filter ratio (temperature) profiles in comparison with the predictions of static-equilibrium theory. It has been suggested that mass flows may explain these discrepancies. We investigate this conjecture using one-dimensional hydrodynamic simulations of steady flows in coronal loops. The flows are driven by asymmetric heating that decreases exponentially along the loop from one footpoint to the other. We find that a sufficiently large heating asymmetry can produce density enhancements consistent with a sizable fraction of the observed loops, but that the pressure scale heights are smaller than the corresponding gravitational scale heights, and that the filter ratio profiles are highly structured, in stark contrast to the observations. We conclude that most warm EUV loops cannot be explained by steady flows. It is thus likely that the heating in these loops is time dependent.

Subject headings: hydrodynamics — Sun: corona — Sun: UV radiation

1. INTRODUCTION

Solar active regions (ARs) are areas of enhanced magnetic field on the Sun that are threaded by numerous coronal loops emitting at EUV and soft X-ray (SXR) wavelengths (e.g., Bray et al. 1991). These loops are magnetic flux tubes connecting opposite-polarity patches in the photosphere that are loaded with hot coronal plasma. They are the basic building blocks of active regions. Since EUV and SXR emissions affect the chemistry and dynamics of the terrestrial atmosphere, understanding how loops are heated to million degree temperatures is a cornerstone problem for both solar physics and the discipline of Sun-Earth connections.

Recent observations and modeling of EUV loops have revealed several very puzzling properties (e.g., Lenz et al. 1999; Aschwanden, Schrijver, & Alexander 2001; Winebarger, Warren, & Mariska 2003). It is now clear that a majority of these loops cannot be explained by static-equilibrium theory (e.g., Rosner, Tucker, & Vaiana 1978; Serio et al. 1981), which has proved so successful in explaining many aspects of SXR loops. In this theory, loops are steady (time-independent) structures characterized by force and energy balance in the absence of flow. They are obviously in hydrostatic equilibrium.

The new EUV observations were made by the multilayer telescopes on the *Transition Region and Coronal Explorer* (*TRACE*) and *Solar and Heliospheric Observatory* (*SOHO*; EUV Imaging Telescope [EIT]) spacecraft. Both instruments have three channels (171, 195, and 284 Å) with maximum temperature sensitivity in the range $\approx$ 1–2 MK. The ratio of intensities observed in two channels, often called a filter ratio, is an indication of the plasma temperature, under the assumption that the plasma is isothermal within the observational pixel. Most EUV loops have a nearly constant 195 : 171 Å ratio along their entire length, suggesting a uniform temperature of $\approx$1.2 MK (e.g., Aschwanden et al. 1999; Aschwanden, Nightingale, & Alexander 2000; Lenz et al. 1999). This is generally inconsistent with static-equilibrium theory, which predicts that temperature should rise abruptly in the transition region and then more slowly, but significantly, in the corona.

A second inconsistency concerns the visibility of EUV loops at great heights above the solar surface. The loops can be very long and high arching, with heights as much as 4 times the pressure scale height for a plasma in hydrostatic equilibrium at $\approx$1.2 MK (Aschwanden et al. 2001). The brighter-than-expected emission at these altitudes indicates pressure gradients that are much shallower than those for a plasma in hydrostatic equilibrium. Direct measurements of the pressure scale height find it to be typically 2–4 times larger than the gravitational scale height.

A third inconsistency concerns loop densities. From the observed intensity, temperature (as inferred from the filter-ratio method), and diameter of a loop, a lower limit on the density can be inferred by assuming that the loop is completely filled (i.e., it has a filling factor of unity). The density limits obtained from *TRACE* observations indicate that loops are overdense by factors of 2–2000 compared to static equilibrium (Winebarger et al. 2003). Small filling factors make the discrepancy even worse. Let us mention here that the filter-ratio method used to derive temperatures suffers from significant ambiguities, and by no means leads to a unique solution (e.g., Testa et al. 2002).

To summarize, in comparison with the predictions of static-equilibrium theory, warm ($\approx$1 MK) EUV loops generally have

[1] Also at: Center for Earth Observing and Space Research, Institute for Computational Sciences, George Mason University, Fairfax, VA 22030.

(1) enhanced densities, (2) enhanced pressure scale heights, and (3) flat filter ratios. Detailed modeling shows that the density and filter-ratio discrepancies can be reduced if the coronal heating is assumed to be concentrated low in the legs of the loops. However, reasonable agreement can be obtained for only about 30% of observed cases (Aschwanden et al. 2001; Winebarger et al. 2003). More than two-thirds of EUV loops are incompatible with static-equilibrium theory, even with footpoint heating. The filter ratio functions for *TRACE* are not single valued, i.e., a particular value of the ratio can correspond to more than one temperature. In interpreting the observations, it is customary to assume the temperature at which the instrument is most sensitive. However, it has been suggested that the loops observed by *TRACE* may actually be much hotter, in which case the discrepancies with static equilibrium would be considerably reduced (Reale & Peres 2000). This is an intriguing possibility. Such hot loops would be easily detectable by the Soft X-ray Telescope on *Yohkoh*, and would produce intense *TRACE*-detectable emission at their transition region footpoints, and there is some question as to whether such observational signatures are present in the data.

Given the shortcomings of a static-equilibrium interpretation, an obvious next step is to consider the possibility of steady flows. Indeed, there exists observational evidence for the existence of substantial mass flows in active regions. Spectroscopic observations of shifts in the spectral line profiles averaged over large areas in active regions or at the footpoints of loops imply line-of-sight velocities of the order of 20 km s^{-1} (e.g., Klimchuk 1987; Kjeldseth-Moe & Brekke 1998; Teriaca, Banerjee, & Doyle 1999; Spadaro et al. 2000; Winebarger et al. 2002). Furthermore, *TRACE* observations of slowly (5–20 km s^{-1}) moving intensity fronts at the feet of large-scale coronal loops could be another manifestation of mass flows (Winebarger, DeLuca, & Golub 2001).

At this point, it is useful to review some of the basic physical properties of loops with flows (see also Bray et al. 1991). The presence of flow in a loop can affect both the energetics (i.e., thermal structure) and dynamics (i.e., pressure structure). Loop energetics are modified by the flow-related terms (enthalpy, and kinetic and gravitational energy) in the energy-balance equation, as well as by the specific spatial form of the heating invoked to drive the flow. Loop dynamics are modified by the ram-pressure term in the momentum balance equation. However, because the hydrodynamic equations represent a set of coupled and nonlinear differential equations, the dynamical and energetic aspects of loops are interconnected.

Steady mass flows have been extensively modeled in the past. In many studies, the flows are driven by a prescribed gas pressure difference at the two footpoints (e.g., Cargill & Priest 1980; Noci 1981; Robb & Cally 1992; Orlando, Peres, & Serio 1995a, 1995b; Betta et al. 1999). Such an approach is realistic if one takes the footpoints to be located in the photosphere or below, because there the plasma β is larger than unity, and gas pressure differences may be required to offset magnetic pressure differences in order to have lateral force balance. For example, if one footpoint of a loop is wider than the other, it has a weaker field strength and must therefore have a higher gas pressure.

This argument does not apply in the chromosphere and transition region, where the β is small and the plasma plays no significant role in the lateral force balance. In this region, it may not be appropriate to specify a pressure boundary condition. The pressure at the top of the chromosphere and above depends sensitively on the heating and energy balance throughout the loop. A realistic model should therefore treat the pressure as a free parameter. If it does not, the resulting solution may imply conditions at and below the footpoint that are difficult to justify. In some situations, solutions may not exist (Mariska & Boris 1983; Betta et al. 1999).

The most physically straightforward way to generate steady flows in coronal loop models is to specify a heating *asymmetry*, so that one side of the loop receives a greater energy input than the other (e.g., Boris & Mariska 1982; Mariska & Boris 1983; Craig & McClymont 1986; Betta et al. 1999). Pressure differences at the footpoints result, but it is clear how the differences arise. Winebarger et al. (2002) have recently shown that a steady-flow solution of this type has 3 times higher densities and a flatter filter ratio profile than the corresponding static solution with the same peak temperature. It therefore agrees better with the observations of EUV loops. The goal of the present work is to further investigate this encouraging development, and to determine whether EUV loops can be explained with steady flows generated by heating asymmetries.

This paper is organized as follows: in § 2 we describe the numerical code we used to solve the one-dimensional hydrodynamic equations; in § 3 we describe the details of our simulations; and in § 4 we present our results. We conclude with a discussion and conclusions in § 5.

2. NUMERICAL MODEL

Given the fact that the solar corona is a highly conducting low-β medium, the magnetic field confines the plasma within flux tubes, and the plasma can be described with one-dimensional hydrodynamics. The time-dependent single-fluid equations for conservation of mass, momentum, and energy along a coronal loop are

$$\frac{\partial \rho}{\partial t} + \frac{\partial}{\partial s}(\rho v) = 0, \tag{1}$$

$$\frac{\partial}{\partial t}(\rho v) + \frac{\partial}{\partial s}(\rho v^2) = \rho g_{\parallel}(s) - \frac{\partial P}{\partial s}, \tag{2}$$

$$\frac{\partial E}{\partial t} + \frac{\partial}{\partial s}[(E+P)v] = \rho v g_{\parallel}(s) + \frac{\partial}{\partial s}\left(k_0 T^{5/2}\frac{\partial T}{\partial s}\right) - n^2\Lambda(T) + H, \tag{3}$$

and

$$E = \frac{1}{2}\rho v^2 + \frac{P}{\gamma - 1}, \tag{4}$$

where we have assumed that loops have a constant cross section, as supported by observations of both EUV and SXR loops (Watko & Klimchuk 2000; Klimchuk 2000). In the above equations, s corresponds to the distance along the loop from the "left" base of the model; $\rho = 1.67 \times 10^{-24} \times n$ is the mass density assuming a fully ionized hydrogen plasma, with n being the electron number density; v is the plasma flow velocity; T is the plasma temperature; $P = 2nkT$ is the pressure from the ideal gas law; $\kappa_0 = 10^{-6}$ is the coefficient of thermal conduction; $\gamma = 5/3$ is the ratio of the specific heats; H is the volumetric heating rate; $\Lambda(T)$ is the optically thin radiation-loss function; and $g_{\parallel}(s)$ is the component of gravity

parallel to the loop axis. We do not include compressive viscosity in equations (2) and (3), which can be important during the early stages of solar flares, when shocks develop (e.g., Peres & Reale 1993), but which is not significant in the steady-flow simulations presented here.

The coronal part of our loop is taken to be semicircular, with a full length $L = 300$ Mm, typical of observed EUV loops. We account for the decrease in gravitational acceleration with distance from Sun center, and therefore $g_{\|}(s) \equiv g_{\odot}\{R_{\odot}[R_{\odot} + h(s)]^{-1}\}^2 \cos[\theta(s)]$, where $h(s)$ is the height above the solar surface, $g_{\odot}$ is the gravitational acceleration at the surface, $R_{\odot}$ is the solar radius, and $\theta(s)$ is the angular position along the semicircle. Attached to each end of the coronal semicircle is a 60 Mm chromospheric section. The total length of the model flux tube is therefore 420 Mm.

We adopt an optically thin radiative loss function $\Lambda(T)$ that has a piecewise continuous power-law form as given in Klimchuk & Cargill (2001). It is based on atomic physics calculations of J. Raymond (1994, private communication), and uses abundances that are a factor of 2 greater than the Meyer (1985) coronal values. The loss function drops precipitously to zero between 30,000 and 29,500 K, guaranteeing that the model chromosphere is approximately isothermal within this temperature range. A more realistic treatment would require optically thick radiative transfer and is unnecessary for studying the properties of the coronal part of the loop. All that we demand of the chromosphere is that it provide a source and sink of mass through the processes of chromospheric evaporation and condensation.

Equations (1) to (3) are solved using our state-of-the-art one-dimensional hydrodynamic code, Adaptively Refined Godunov Solver (ARGOS), which is described in detail in Antiochos et al. (1999). Two aspects of ARGOS make it particularly well suited for studying coronal and transition-region dynamics. First, the time-dependent solution is advanced using a second-order Godunov scheme with a Monotone Upwind Schemes for Scalar Conservation Laws (MUSCL) limiter, which is one of the most robust numerical schemes for studying one-dimensional hydrodynamics. Second, ARGOS employs the PARAMESH parallel adaptive mesh refinement (AMR) package, which dynamically refines or "derefines" the grid based on the local density variations. For the applications described in this paper, the minimum grid spacing is roughly 25 km, which is adequate for resolving the small spatial scales of the transition region. Rigid wall boundary conditions are applied at the ends of the flux tube. Our model chromosphere is many gravitational scale heights thick [$H_g(T = 30,000\ \mathrm{K}) \approx 1500$ Mm], so that the boundary conditions have negligible influence on the plasma dynamics in the transition region and corona, and so that the height of the chromosphere is not affected by the depletion and accumulation of mass.

3. DETAILS OF THE HYDRODYNAMIC SIMULATIONS

As a first step, we calculated a static-equilibrium solution to serve as a reference for comparison with the steady-flow solutions. We accomplished this by prescribing a spatially uniform heating rate of $H = 4.6 \times 10^{-6}$ ergs cm^{-3} s^{-1} and allowing an initial approximate equilibrium based on scaling-law theory (e.g., Rosner et al. 1978; Serio et al. 1981), to relax to the true equilibrium. The relaxation was terminated when the residual mass motions had diminished to less than 0.5 km s^{-1}. The relaxed static equilibrium has an apex temperature of approximately 1.2 MK, typical of loops observed by *TRACE*.

We then carried out a series of steady-flow simulations for the same loop. Beginning with the static solution, we modified the heating so that it decreases exponentially along the loop from one footpoint all the way to the other footpoint,

$$H(s) = H_0 \ \exp\left(-\frac{s - s_{\mathrm{base}}}{s_H}\right), \tag{5}$$

where s_H is the heating scale length and H_0 is the magnitude of the heating at s_{base}, the position of the top of the chromosphere (i.e., base of the corona) on the "left" side of the static solution. Note that the heating does *not* increase with height on the "right" side, as it does in the steady solution of Winebarger et al. (2002) and the thermal nonequilibrium solutions of Karpen et al. (2001, 2003). Note also that the static solution can be regarded as a special case of the exponential heating function when s_H tends to infinity.

For a given choice of s_H and H_0, we kept the heating constant in time and allowed the solution to relax to a steady equilibrium. Transient flows and sound waves are initially excited, but after a few tens of thousands of seconds, corresponding to several sound crossing times (of the order of few 1000 s) across the system, all the physical parameters vary by less than 1% throughout the loop. We nonetheless continued the calculations for an additional $\approx$100,000 s to verify that the solution is stable.

We considered three different values for s_H, corresponding to progressively more asymmetric heating: $s_H = L/10$, $L/20$, and $L/40$. For each, we found a different H_0 (1.5×10^{-4}, 6.5×10^{-4}, and 17.5×10^{-4} ergs cm^{-3} s^{-1}, respectively) such that the peak temperature approximately matches the 1.2 MK peak temperature of the static solution. We discovered that the total heating integrated along the loop, $H_{\mathrm{tot}} \equiv \int_{\mathrm{loop}} H(s)\, ds$, is a *decreasing* function of s_H. In other words, smaller heating scale lengths require more total energy to produce the same peak temperature. This has important consequences for the loop density, as we discuss later.

The exponential heating function of equation (5) applies throughout the loop, including the chromosphere. Different models therefore have different chromospheric heating rates. However, because our radiation-loss function is extremely steep between 2.95×10^4 and 3.0×10^4 K, large changes in the heating rate are offset by very small changes in temperature, and the structure of the chromosphere is nearly identical in all of the models. The height of the chromosphere varies slightly from model to model because of differences in the coronal (and transition region) pressure. For example, the top of the chromosphere in the $s_H = L/40$ model is displaced by approximately 3000 km compared to the static model. This is an entirely physical effect that we expect to occur on the Sun.

4. RESULTS

4.1. *Flow Velocities*

The flow velocities along the loop for the three steady solutions are shown in Figure 1. The velocities are positive throughout the loop, which means that they are upward in the left half and downward in the right half. The flows are driven by a pressure imbalance associated with the asymmetric heating. Greater heating on the left side produces enhanced pressure compared to the right side. We can easily understand

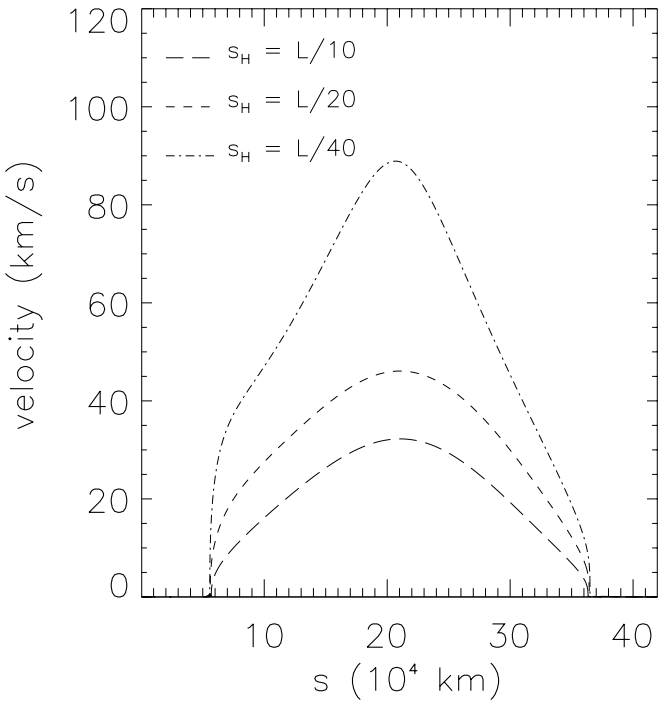

FIG. 1.—Flow velocity vs. position along the loop for the steady solutions, with $s_H = L/10$ (*long-dashed line*), $L/20$ (*short-dashed line*), and $L/40$ (*dash-dotted line*). Positive velocities correspond to upflow in the left half of the loop and downflow in the right half.

this by considering the static loop scaling law (e.g., Rosner et al. 1978)

$$P \propto H^{6/7} L^{5/7}, \tag{6}$$

which can be applied separately to the left and right sides of the loop. Since L is the same on both sides, if H is greater on the left, P must be also greater. This implies that a static state is not possible, and a flow is set up from left to right. We see from Figure 1 that larger heating asymmetries (smaller s_H) produce greater velocities. This is expected, since the pressure asymmetries are correspondingly larger. We note that the velocities are subsonic for all the three cases considered here (the sound speed at a temperature of 1.2 MK is $\approx$160 km s^{-1}), although they correspond to a significant fraction of the sound speed, with a maximum Mach number $M \approx 0.7$.

4.2. *Densities*

The densities along the loop for the static solution and the three steady-flow solutions are shown in Figure 2. The flow solutions have higher densities, with the density increasing for greater heating asymmetry. Compared to the static solution, the apex densities are enhanced by factors of $\approx$3, 6, and 7 for $s_H = L/10, L/20$, and $L/40$, respectively. The enhancements are less in the lower sections of the loop.

As mentioned earlier, and for reasons we discuss shortly, loops with asymmetric heating require more total energy to have the same peak temperature as uniformly heated loops. This implies higher densities, since loops lose energy almost exclusively by radiation, and the radiative output scales with the square of the density. Thermal conduction and flows are energetically important, but they serve only to redistribute energy between the corona and transition region, and between different parts of the corona (see the Appendix).

4.3. *Pressures*

Pressures are also enhanced in the steady-flow solutions, as shown in Figure 3. The enhancement generally increases with increasing heating asymmetry, although at the apex the trend reverses between $s_H = L/20$ and $L/40$, because of a temperature inversion discussed below. The maximum pressure enhancement in our solutions is a factor of $\approx$6.

Equally important from an observational standpoint is the fact that, in the coronal section of the loop, the flow solutions have pressure scale heights that are *shorter* than the local gravitational scale height, $H_P < H_g(T)$, where $H_P = P|\partial P/\partial z|^{-1}$ and z is the vertical coordinate. In the static solution, the pressure gradient need only be large enough to support the weight of the plasma, but in the flow solutions, it must be greater in order to accelerate the plasma on the left side and decelerate the plasma on the right side. It is straightforward to show that for subsonic mass flows $H_P/H_g \approx 1 - \gamma M^2$, where M is the Mach number. The exact ratio H_P/H_g, together with its approximation given above, is plotted in Figure 4 as a function of position along the loop for the $s_H = L/40$ model.

4.4. *Temperatures and Filter Ratios*

The temperature profiles for the static and steady-flow solutions are shown in Figure 5. As the heating asymmetry increases, the temperature profile first flattens and then develops a minimum near the apex, which becomes progressively deeper. Similar behavior is found for heating that is concentrated symmetrically near the footpoints of both legs (e.g., Aschwanden et al. 2001; Winebarger et al. 2003). The reason is as follows. With uniform heating, there is enough energy deposited at the apex to power the local radiative losses. In fact, there is too much energy, and roughly half is conducted down the legs to be radiated from the transition

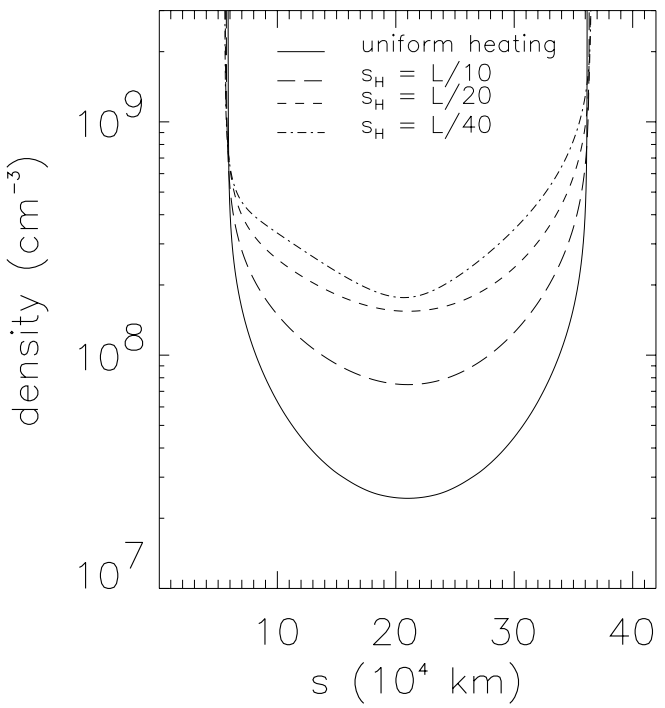

FIG. 2.—Electron number density vs. position along the loop for the static solution (*solid line*), and steady-flow solutions with $s_H = L/10$ (*long-dashed line*), $L/20$ (*short-dashed line*), and $L/40$ (*dash-dotted line*).

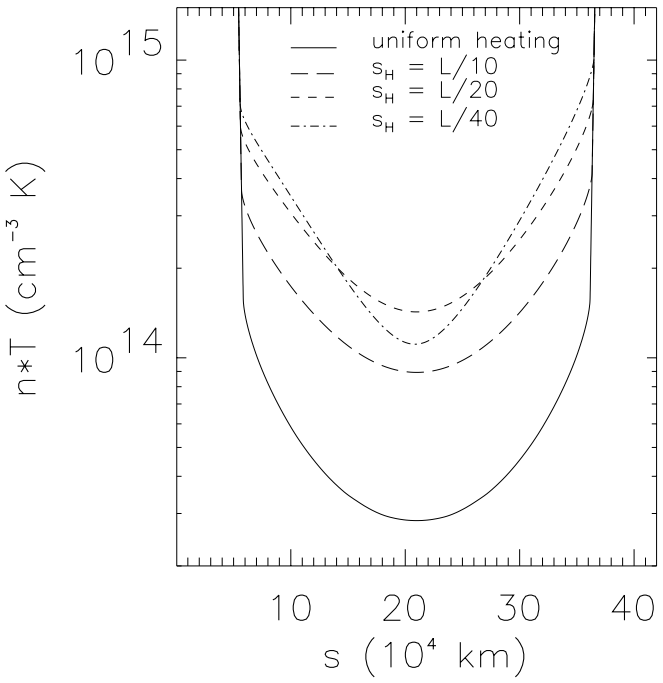

FIG. 3.—Plot of $n \times T$ ($\propto$ pressure) vs. position along the loop for the static solution (*solid line*), and steady-flow solutions with $s_H = L/10$ (*long-dashed line*), $L/20$ (*short-dashed line*), and $L/40$ (*dash-dotted line*).

region (Vesecky, Antiochos, & Underwood 1979). With a heating profile that decreases exponentially with height, comparatively less energy is deposited at the apex, and the thermal conduction losses must be reduced. These losses vary as $T^{5/2}dT/ds$, so both the temperature and temperature gradient decrease. The temperature profile flattens and shrinks.

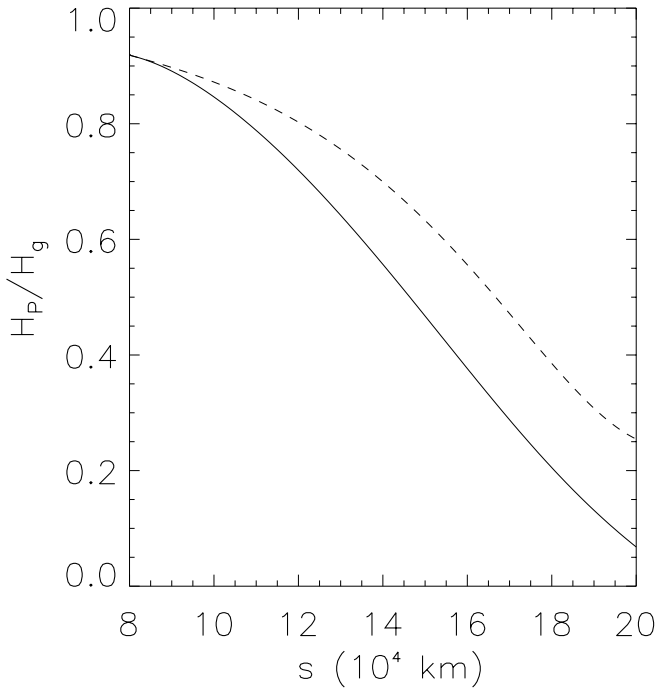

FIG. 4.—Ratio $H_P : H_g$ of the pressure scale height to the local gravitational scale height in a coronal section of the loop for the steady-flow model with $s_H = L/40$, showing the exact ratio (*solid line*) and the analytical approximation given in § 4.3 (*dashed line*).

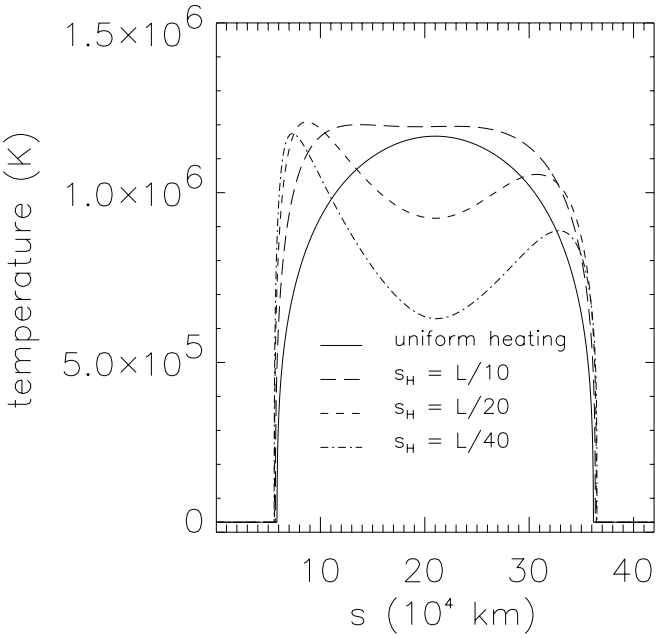

FIG. 5.—Temperature vs. position along the loop for the static solution (*solid line*), and steady-flow solutions with $s_H = L/10$ (*long-dashed line*), $L/20$ (*short-dashed line*), and $L/40$ (*dash-dotted line*).

Increasing the heating throughout the loop (i.e., increasing H_0) raises the peak temperature back up to its uniform heating value, but the temperature profile remains flattened. For sufficiently small scale lengths ($s_H < L/10$), the energy deposited at the apex is so small that thermal conduction must switch from a cooling mechanism to a heating mechanism, and a temperature inversion develops (see also Betta et al. 1999).

This argument applies to loops with heating concentrations in one or both footpoints. In the former case, studied here, there is little energy deposited anywhere in the right leg. Energy associated with the flow must supplement or replace thermal conduction in order to power the radiative losses on that side. On the left side, the flow acts primarily as a cooling mechanism. Thus, the primary role of the flow is to transfer energy from the left side of the loop, which receives most of the coronal heating, to the right side. Both sides radiate strongly. Figure 6 shows profiles of the different terms of the energy equation for the case of intermediate heating asymmetry. Positive values represent energy sources and negative values represent energy sinks. The net is zero, as it must be for a loop in equilibrium. Note that kinetic energy is unimportant compared to enthalpy, since the flows are subsonic.

The ratio of the intensities that would be observed in the 195 and 171 Å channels of *TRACE* are shown in Figure 7. These intensities are equal to the product of the emission measure and the temperature-dependent response function for each channel. The intensity ratio reduces to the ratio of the corresponding response functions. We used the response functions provided in the SolarSoft package, which were calculated using version II of the CHIANTI atomic database. The calculations assume coronal abundances (Feldman 1992) and ionization equilibrium from the calculations of Arnaud & Raymond (1992). We see that the intensity-ratio profiles have a similar appearance to the temperature profiles. This results from the fact that the response functions are sharp functions of temperature. The profile is rather flat for the mildest heating asymmetry we have considered, but it is highly structured in

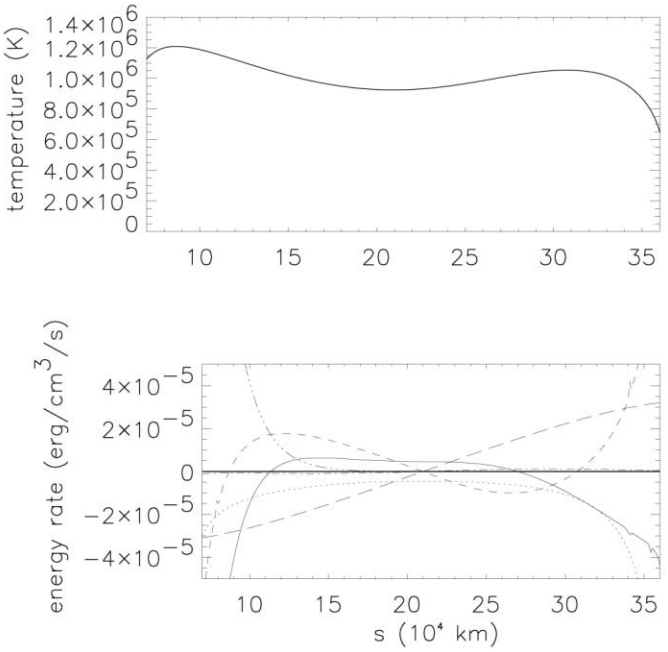

FIG. 6.—Temperature (*top panel*) and sources and sinks of energy (*bottom panel*) vs. position along a central section of the loop for the steady-flow solution with $s_H = L/20$, showing thermal conduction (*solid line*), gravitational energy (*long-dashed line*), enthalpy (*short-dashed line*), radiation (*dotted line*), kinetic energy (*dash-dotted line*), and heating $H(s)$ (*dash–triple-dotted line*). The energies sum to zero, as indicated by the thick solid line. The loop apex is at $s = 21 \times 10^4$ km.

the other two cases. The ratio varies across each leg by nearly 1 order of magnitude for $s_H = L/20$, and by nearly 2 orders of magnitude for $s_H = L/40$. The "spikes" at the ends occur in the thin transition region.

5. DISCUSSION AND CONCLUSIONS

We now address whether our steady-flow models are consistent with the observations of warm (≈1 MK) EUV loops. Recall that observed loops generally have higher densities, larger pressure scale heights, and flatter filter ratios than predicted by static-equilibrium models. On the first point, our models represent an improvement over the static models. The factor of 7 density enhancement in the case $s_H = L/40$ is adequate to explain a considerable fraction of the *TRACE* loops studied by Winebarger et al. (2003). Unfortunately, that model has a highly structured filter-ratio profile that is entirely incompatible with the observations (Lenz et al. 1999). The model with mild heating asymmetry ($s_H = L/10$) successfully reproduces the observed filter ratios, but it predicts a density enhancement of only a factor of 3, which is too small for a large majority of the *TRACE* loops. Finally, the flow models have pressure scale heights that are smaller than the gravitational scale heights of static equilibrium, which is opposite to what is observed. We must conclude that warm EUV loops cannot be explained by steady flow models of the type we have considered. We note here that steady flow models are also unable to explain cool ($T < 10^6$ K) loops (e.g., Peres & Orlando 1996; Peres 1997) reported by Foukal (1976).

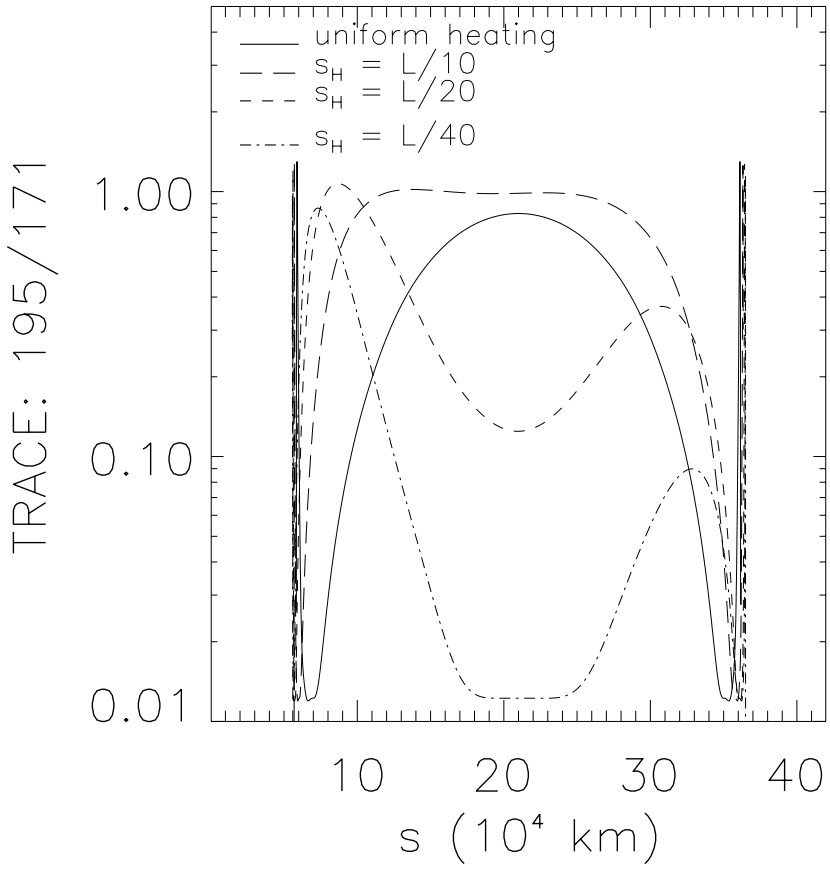

FIG. 7.—Ratio of intensities in the *TRACE* 195 and 171 Å channels vs. position along the loop for the static solution (*solid line*), and steady-flow solutions with $s_H = L/10$ (*long-dashed line*), $L/20$ (*short-dashed line*), and $L/40$ (*dash-dotted line*). The distance between the tick marks (i.e., 10 Mm) corresponds to ≈ 25 *TRACE* pixels.

If static and steady-flow models are unable to explain the loops, it must be that either the models are missing some important physics or the loops are heated in a time-dependent manner. Missing physics could include the pressure force associated with propagating waves (Woods, Holzer, & MacGregor 1990; Hollweg 1981) or standing waves (Litwin & Rosner 1998). We find the idea of time-dependent heating very appealing, since we are aware of no plausible heating mechanism that would produce steady heating on a given magnetic field line. Furthermore, impulsively heated loops have enhanced densities when their temperatures are in the range detectable by *TRACE* (e.g., Cargill & Klimchuk 1997; Warren, Winebarger, & Hamilton 2002; Spadaro et al. 2003). A number of independent lines of evidence now point to a picture in which loops comprise multiple unresolved strands that are heating by nanoflare–like energy bursts, as advocated by Cargill (1994) and others. We are actively pursuing detailed models of this type, and will report on the results of our study in a future article. In principle, the strands of a multistranded loop could contain steady flows, but we would not expect such a loop to agree significantly better with the observations than a single monolithic loop.

An alternative to impulsive heating is heating that is steady for a considerable period and then suddenly switches off (see also Reale & Peres 2000). Such a scenario might explain the enhanced densities seen by *TRACE*, but only if the initial loop temperature (the temperature before the heating decrease) is much hotter than 1 MK.

We close by comparing our steady-flow models with models in which the heating decreases exponentially with height in *both* legs. First, consider the symmetric case of equal heating in both legs. Several studies have shown that a stable equilibrium is possible only if the heating scale length is not too small compared to the loop length. The requirement is that $s_H > L/6$, approximately, where the reader is reminded that L is the total loop length (Serio et al. 1981; Aschwanden et al. 2001; Sigalotti & Mendoza-Briceno 2003; Winebarger et al. 2003). These symmetric equilibria are necessarily static. In contrast, we find stable equilibria with flows when s_H is at least as small as $L/40$. The difference demonstrates the importance of the flows to the local energy balance.

In time-dependent calculations of symmetric heating with s_H less than the critical value for equilibrium, a cool condensation forms and grows at the top of the loop (Antiochos & Klimchuk 1991; Antiochos et al. 1999). In principle, the loop can reach equilibrium once the condensation becomes sufficiently large (Dahlburg, Antiochos, & Klimchuk 1998), although we would only expect this to occur under special circumstances. If a mild asymmetry is introduced, so that the exponential heating is slightly (~25%) stronger in one leg than the other, a phenomenon know as "thermal nonequilibrium" occurs (Antiochos, MacNeice, & Spicer 1999; Karpen et al. 2001, 2003). Instead of a steady flow developing, as in our models, condensations form and fall down the more weakly heated leg in a never-ending cycle. We can understand the different behavior as follows: strong footpoint heating drives evaporative upflows in both legs; because the upflows are comparable, mass collects at the top where the upflows collide, until a radiative instability ultimately produces a condensation. In our models, the heating is orders of magnitude stronger in one leg than the other. The upflow from that leg dominates, and a unidirectional flow is rapidly established. It appears, therefore, that thermal nonequilibrium requires not only a small heating scale length, but also a sufficiently mild heating asymmetry. Quantifying this assertion must await additional detailed modeling.

This work was supported by NASA and the Office of Naval Research. We thank Spiro Antiochos, Markus Aschwanden, Judith Karpen, John Mariska, Giovanni Peres, Gordon Petrie, Fabio Reale, Sarah Tanner, Harry Warren, and Amy Winebarger for helpful discussions and comments. Spiros Patsourakos wishes to thank Sevasti Zoumi for encouragement.

APPENDIX

EQUILIBRIUM LOOP ENERGY LOSSES

Flows and thermal conduction play important roles redistributing energy within an equilibrium loop, either between the corona and transition region, or between different parts of the corona. They are not, however, significant in the global energy budget of the loop as a whole. Equilibrium loops gain energy almost exclusively by coronal heating, and lose energy almost exclusively by radiation. In the following discussion, we take the loop footpoint to be the top of the chromosphere, which has a temperature of 3×10^4 K in our models.

The flux of energy carried by thermal conduction is

$$F_c = \kappa_0 T^{5/2} \frac{dT}{ds}. \tag{A1}$$

Since the temperature gradient vanishes at the top of the chromosphere (approximately), there is minimal flow of energy through the footpoint.

Flows carry enthalpy, gravitational energy, and kinetic energy. The enthalpy flux is

$$F_e = \frac{\gamma}{\gamma - 1} Pv = \frac{\gamma R}{\gamma - 1} T(\rho v), \tag{A2}$$

where γ is the ratio of specific heats and R is the ideal gas constant. Since the mass flux ρv is constant throughout the loop and T is the same at both footpoints, F_e must also be the same at both footpoints. A given sign of F_e represents inflow at one footpoint and outflow at the other, so there is no net change in the energy of the loop. Similarly, the gravitational energy flux,

$$F_g = g_{\parallel}(\rho v), \tag{A3}$$

makes no net energy contribution as long as the loop has the same inclination at both footpoints. The kinetic-energy flux,

$$F_k = \frac{1}{2}\rho v^3 = \frac{1}{2}v^2(\rho v), \tag{A4}$$

is not necessarily the same at both footpoints. However, because the flows are highly subsonic at the footpoints, the energy flux is insignificant compared to the coronal heating and radiation integrated along the loop. It does not impact the global energy budget of the loop.

REFERENCES

Antiochos, S. K., & Klimchuk, J. A. 1991, ApJ, 378, 372
Antiochos, S. K., MacNeice, P. J., Spicer, D. S., & Klimchuk, J. A. 1999, ApJ, 512, 985
Arnaud, M., & Raymond, J. C. 1992, ApJ, 398, 394
Aschwanden, M. J., Newmark, J. S., Delaboudiniere, J. P., Neupert, W. M., Klimchuk, J. A., Gary, G. A., Portier-Fornazzi, F., & Zucker, A. 1999, ApJ, 515, 842
Aschwanden, M. J., Nightingale, R. W., & Alexander, D. 2000, ApJ, 541, 1059
Aschwanden, M. J., Schrijver, C. J., & Alexander, D. 2001, ApJ, 550, 1036
Betta, R., Peres, G., Serio, S., & Orlando, S. 1999, in Proc. Magnetic Fields and Solar Processes, 9th European Meeting on Solar Physics, ed. A. Wilson (ESA SP-448; Noordwijk: ESA), 475
Boris, J. P., & Mariska, J. T. 1982, ApJ, 258, L49
Bray, R. J., Cram, L. E., Durrant, C. J., & Loughhead, R. E. 1991, Plasma Loops in the Solar Corona (Cambridge: Cambridge Univ. Press)
Cargill, P. J. 1994, ApJ, 422, 381
Cargill, P. J., & Klimchuk, J. A. 1997, ApJ, 478, 799
Cargill, P. J., & Priest, E. R. 1980, Sol. Phys., 65, 251
Craig, I. J. D., & McClymont, A. N. 1986, ApJ, 307, 367
Dahlburg, R. B., Antiochos, S. K., & Klimchuk, J. A. 1998, ApJ, 495, 485
Feldman, U. 1992, Phys. Scr., 46, 202
Foukal, P. 1976, ApJ, 210, 575
Hollweg, J. V. 1981, Sol. Phys., 70, 25
Karpen, J. T., Antiochos, S. K., Hohensee, M., Klimchuk, J. A., & MacNeice, P. J. 2001, ApJ, 553, L85
Karpen, J. T., Antiochos, S. K., Klimchuk, J. A., & MacNeice, P. J. 2003, ApJ, 593, 1187
Kjeldseth-Moe, O., & Brekke P. 1998, Sol. Phys., 182, 73
Klimchuk, J. A. 1987, ApJ, 323, 368
———. 2000, Sol. Phys., 193, 53
Klimchuk, J. A., & Cargill, P. J. 2001, ApJ, 553, 440
Lenz, D. D., DeLuca, E. E., Golub, L., Rosner, R., & Bookbinder, J. A. 1999, ApJ, 517, L155
Litwin, C., & Rosner, R. 1998, ApJ, 506, L143
Mariska, J. T., & Boris, J. P. 1983, ApJ, 267, 409
Meyer, J. P. 1985, ApJS, 57, 173
Noci, G. 1981, Sol. Phys., 69, 63
Orlando, S., Peres, G., & Serio, S. 1995a, A&A, 294, 861
———. 1995b, A&A, 300, 549
Peres, G. 1997 in Proc. 5th *SOHO* Workshop, The Corona and Solar Wind near Minimum Activity, ed. A. Wilson (ESA SP-404; Noordwijk: ESA), 55
Peres, G., & Orlando, S. 1996, in ASP Conf. Ser. 9, Cool Stars, Stellar Systems, and the Sun, ed. G. Wallerstein (San Francisco: ASP), 93
Peres, G., & Reale, F. 1993, A&A, 267, 566
Reale, F., & Peres, G. 2000, ApJ, 528, L45
Robb, T. D., & Cally, P. S. 1992, ApJ, 397, 329
Rosner, R., Tucker, W. H., & Vaiana, G. S. 1978, ApJ, 220, 643
Serio, S., Peres, G., Vaiana, G. S., Golub, L., & Rosner, R. 1981, ApJ, 243, 288
Sigalotti, L. Di G., & Mendoza-Briceno, C. A. 2003, A&A, 397, 1083
Spadaro, D., Lanza, A. F., Lanzafame, A. C., Karpen, J. T., Antiochos, S. K., Klimchuk, J. A., & MacNeice, P. J. 2003, ApJ, 582, 486
Spadaro, D., Lanzafame, A. C., Consoli, L., Marsch, E., Brooks, D. H., & Lang, J. 2000, A&A, 359, 716
Teriaca, L., Banerjee D., & Doyle, J. G. 1999, A&A, 349, 636
Testa, P., Peres, G., Reale, F., & Orlando, S. 2002, ApJ, 580, 1159
Vesecky, J. F., Antiochos, S. K., & Underwood, J. H. 1979, ApJ, 233, 987
Warren, H. P., Winebarger, A. R., & Hamilton, P. S. 2002, ApJ, 579, L41
Watko, J. A., & Klimchuk, J. A. 2000, Sol. Phys., 193, 77
Winebarger, A. R, DeLuca, E. E., & Golub, L. 2001, ApJ, 553, L81
Winebarger, A. R., Warren, H. P., & Mariska, J. T. 2003, ApJ, 587, 439
Winebarger, A. R., Warren, H. P., van Ballegooijen, A., DeLuca, E. E., & Golub, L. 2002, ApJ, 567, L89
Woods, D. T., Holzer, T. E., & MacGregor, K. B. 1990, ApJS, 73, 489